Papers

Transformation of the Vistula Lagoon onto a canonical domain

Motto:

Il est vrai que le monde visible seroit plus parfeit, si le terres & le mers faisoient de figure plus juste.

(Malebranche 1707)

WŁODZIMIERZ J. PROSNAK
PAWEŁ P. CZEŚNIK
Institute of Oceanology,
Polish Academy of Sciences,
Powstańców Warszawy 55, PL–81–712 Sopot, Poland;
e-mail: czesiek@iopan.gda.pl

Abstract

The paper deals with the conformal mapping of finite, plane, simply connected domains, representing oceans, lakes, estuaries, bays, lagoons, and other natural water bodies of this kind. As a rule, they are bounded by geometrically complex shorelines. The partial differential problems investigated in Oceanology and posed in such domains have turned out to be difficult to solve for at least three reasons.

They follow on from the mathematical properties of the differential equations governing such problems, from the just-mentioned geometrical complexity of the domains of solution, and from the sensitivity of the solutions to boundary conditions.

In view of the last reason the contours admitted as boundaries of the domains of the solution ought to be as close to the real shorelines as possible. The obviously inaccurate approximation of the shorelines by 'staircases', which appears rather often (cf. Catewicz & Jankowski 1983, Lin & Chandler-Wilde 1996) as a consequence of applying finite difference methods to the solution of the partial differential problems, raises serious doubts from the point of view of Numerical Fluid Mechanics.

It is recalled in the paper that such inaccuracies are not unavoidable: that complicated plane domains can be transformed accurately by means of properly applied *conformal mapping* onto regular, canonical domains – in particular, onto discs or squares. Such a transformation is demonstrated on the rather difficult example of the Vistula Lagoon. The transformation begins with the decomposition of the domain into five plane subdomains, each one of which is eventually transformed onto a disc. Every such result is arrived at quite independently of the remaining subdomains, by means of a set of properly selected consecutive mappings. Hence, the final *canonical* domain consists in this case of a system of five discs which, however, within the framework of this differential problem, have to be treated as *interconnected*. The interconnections involve images of four segments of straight lines, separating the original subdomains.

The transformations and the resulting canonical domain presented in the paper are intended to be applied to the solution of certain hydrodynamical problems concerning the Vistula Lagoon, which will be published elsewhere.

1. Introduction

Many physical phenomena considered in Oceanology can be described in the language of mathematics as *partial differential problems* (PDP). Any such problem is defined by a set of partial differential equations and by proper boundary and initial conditions.

Determining the solution to a problem of this kind is rather difficult; it is usually arrived at solely by approximate methods – discrete or analytical-numerical. The difficulties stem from the following properties of the problem:

1. The corresponding set of equations is non-linear; it contains many unknown functions, and up to four independent variables.

2. The solution is sensitive to boundary conditions.

3. The domain of the solution, representing a natural body of water, such as an ocean, a lake, a sea, a bay or a lagoon, is bounded as a rule by a geometrically complex shoreline, and by perhaps not quite so complex a bottom.

The considerations of the present paper will be confined to *plane* problems, in which any function H describing a property of flow may depend on three real arguments:

$$H = H(x, y, t), \tag{1}$$

where x, y, t denote two spatial variables and time, respectively.

The domain of the solution will be regarded as a plane figure bounded by a closed, non-intersecting shoreline.

This domain may contain islands, in which case it is called *multiply* connected; otherwise it is *simply* connected. Only domains of the latter kind will be considered in this paper. It should be stressed, however, that *multiply* connected domains are also covered by existing theory, algorithms and computer programs (Prosnak & Klonowska 1996a), and extension of this research to such domains is perfectly plausible.

The Vistula Lagoon (Fig. 1) may serve as an example of a simply connected domain.
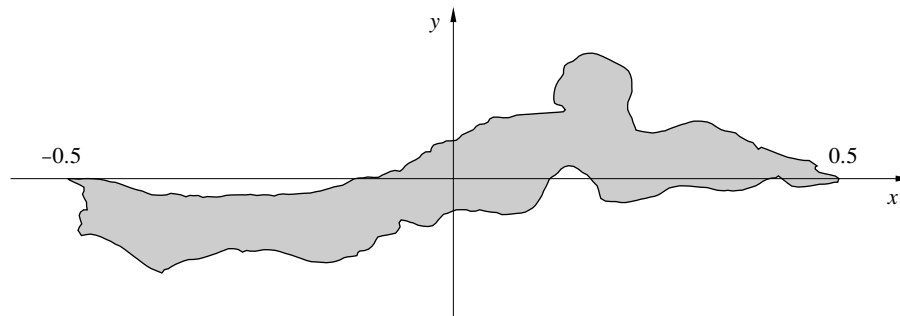
Fig. 1. The Vistula Lagoon

It should be understood that the inlets and the outlets to and from the Lagoon have been disregarded in the Figure, and its chord, situated in the x, y – system of rectangular coordinates, coincides with the segment $(-0.5, +0.5)$ of the axis of the abscissae. Furthermore, the shoreline of the Lagoon is defined by a set of discrete points taken from measurements and extended, if necessary, by interpolated ones.

Such a *true* shoreline appears rather rarely in PDPs of the kind mentioned previously. On the contrary, especially when a finite difference method is applied as a means of arriving at a solution, the true shoreline is replaced by a 'staircase of grid points'. This is the case not only in older papers (see e.g. Catewicz & Jankowski 1983, p. 228), but also in relatively recent ones (e.g. Lin & Chandler-Wilde 1996, Fig. 5). The evident inaccuracy of the boundary must result in defective boundary conditions

and, inevitably, distort the solution of the problem as a whole. (The inaccurate solution may still be of value for some practical applications, but this is another question which will not be taken up in this paper.)

The obvious remedy, already widely applied in other topics of Fluid Mechanics (see Prosnak & Klonowska 1996a, b, Schinzinger & Laura 1991), lies in the various but *exact*, *transformations* of the PDP's under consideration. In the present paper, *transformation of the space variables* will be applied. This leads to the replacement of the given domain of the solution by an auxiliary, *canonical* one, which has a regular boundary and is exemplified by a disc or a square.

The transformation of the original domain of the solution, which is located in the x, y-plane, onto an auxiliary one located in the ξ, η-plane, is represented by a system of two functions:

$$\xi = \xi(x, y); \qquad \eta = \eta(x, y). \tag{2}$$

Solving (2) with respect to x, y yields an equivalent system:

$$x = x(\xi, \eta); \qquad y = y(\xi, \eta), \tag{3}$$

which, inversely, transforms the auxiliary domain onto the original one.

The main benefits arising out of the introduction of the auxiliary domain of the solution can be summarized as follows:

- the regular shape of this domain usually permits the application of *analytical-numerical* methods, in particular of spectral or pseudo-spectral ones, which yields a more economical description of the solution, and sometimes delivers the solution in closed form,

- the regular shape of the lines bounding this domain enables one to impose the boundary conditions very accurately,

- the transformation is *universal*: it does not depend on a particular PDP; it may serve a multitude of such problems posed in the same original domain,

- if the *auxiliary* domain of the solution is represented by a rectangle, the use of purely discrete methods may turn out to be easier.

There is a particular kind of such coordinate transformation called *conformal mapping*. It is widely used for solving the PDP's occurring in various fields of science and technology (for examples, see Prosnak & Klonowska 1996a, b, Schinzinger & Laura 1991). Oceanology seems to represent an exception in this respect, the reason for this undoubtedly stemming from the already mentioned geometrical complexity of the shore line, and of the domain as a whole.

The aims of the present paper are to recall the useful (and beautiful) properties of conformal mapping, and to demonstrate – using the example of

the Vistula Lagoon – that the difficulties of applying this transformation in practice can be surmounted. This finally leads to the sought-after canonical domain in the form of a system of five discs.

No hydrodynamical problem as such will be considered in the paper. It is intended to do so in a separate publication, using the results of the conformal transformation set out in Section 6.

2. Conformal mapping and some of its properties

Definitions. Conformal mapping can be regarded as a special form of transformation of a plane domain onto another one, i.e. as a special form of transforming functions (2) and (3). It makes use of *complex variables*:

$$z = x + iy; \qquad \zeta = \xi + i\eta; \qquad i = \sqrt{-1}, \tag{4}$$

which denote points on the *complex planes* z and ζ, respectively, shown in Fig. 2.
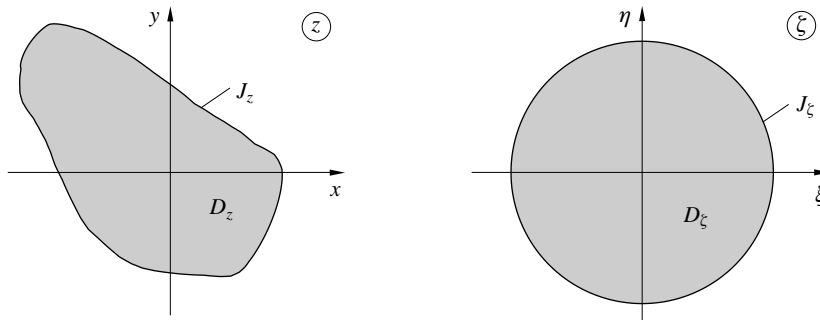
Fig. 2. Conformal mapping of a disc onto a given domain: image and counter image

By virtue of (4) the set of two real functions (3) can be rewritten as

$$z = x(\xi, \eta) + iy(\xi, \eta) = f(\zeta), \tag{5}$$

the symbol ζ denoting the *complex argument*, and z the *complex function*. This function is called *holomorphic* if its *real* and *imaginary parts* satisfy the *Cauchy-Riemann* conditions:

$$\frac{\partial x}{\partial \xi} = \frac{\partial y}{\partial \eta}; \qquad \frac{\partial x}{\partial \eta} = -\frac{\partial y}{\partial \xi}. \tag{6}$$

If a holomorphic function (5) is *univalent* in a domain D_ζ located in the ζ-plane, and exemplified by the disc in Fig. 2, then the function transforms the whole disc together with its bounding circle onto a domain D_z located in the z-plane, and bounded by a *Jordan* curve J_z (Fig. 2). Such a transformation *performed by a holomorphic function* is called *conformal*.

The *Jordan* curve is defined as a closed, non-intersecting line, consisting of a finite number of regular segments. Such a curve with a fixed direction is referred to as the *contour*.

The domains D_z and D_ζ are called the *image* and the *counter-image*, respectively, if the transformation is defined by the function (5).

An example, concerning the *Joukowski* function (Prosnak & Klonowska 1996a)

$$z = \zeta + \frac{c^2}{\zeta}; \qquad c - \text{real}, \tag{7}$$

is given in Fig. 3. The function transforms the infinite exterior of the circle shown in this Figure onto such an exterior of the contour possessing a singular point at

$$x = 2c > 0,$$

the shape and position of this image being defined entirely by function (7), as well as by the radius and center of the circle. By changing the data concerning the circle, one obtains quite different contours. Some typical *Joukowski* contours, as well as examples of given functions different from (7), can be found in Prosnak & Klonowska (1996a).
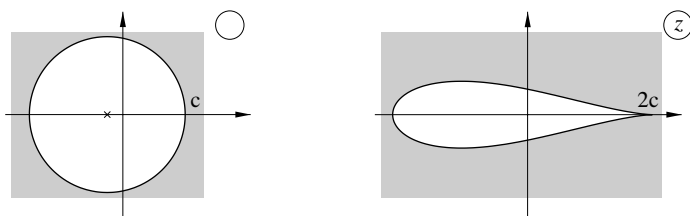
Fig. 3. Conformal mapping of the exterior of a circle onto the exterior of a *Joukowski* profile

Existence and univalence. In the example just presented, the counter-image D_ζ and the mapping function (5) – in the particular form (7) – are given, but the boundary line of the image D_z is not known in advance and has to be evaluated. A much more interesting and, perhaps, even surprising property of the theory of conformal mapping corresponds to the case when, inversely, both the domains D_z and D_ζ are given, *but the mapping function is sought*.

In this paper considerations dealing with such a problem will be confined to *simply connected* domains, both finite and infinite. Moreover, although the two *Jordan* curves bounding the respective domains can be quite arbitrary, one of them will always be assumed to be a circle. Such a domain is usually referred to as *circular*, no matter whether it is finite or infinite.

Under these conditions it can be said that a holomorphic function

$$z = f_{\text{in}}(\zeta), \tag{8}$$

conformally transforming a disc located in the ζ-plane onto an arbitrary *finite* domain located in the z-plane and bounded by a *Jordan* curve, always *exists*, and is *univalent*.

The analogous theorem concerning *infinite*, simply connected domains is true too. This states that a holomorphic function

$$z = f_{\text{ex}}(\zeta), \tag{9}$$

conformally mapping the closed, infinite exterior of a circle onto the closed, infinite exterior of a given arbitrary *Jordan* curve, always *exists*, and is *univalent*.

General forms of the standard mapping functions (8) and (9)

Any holomorphic function defined in a disc can be developed into a power series under certain assumptions relating to the properties of this function. This theorem also applies to the mapping function (8), which can therefore be presented as

$$z = f_{\text{in}}(\zeta) = \sum_{n=0}^{\infty} C_n \left(\frac{\zeta}{A}\right)^n; \qquad |\zeta| \in [0, A], \tag{10}$$

the series converging within the indicated interval, i.e. within the whole, closed disc. The symbol A denotes the radius of the circle, and the symbols

$$C_n; \qquad n = 0, 1, 2, \dots \tag{11}$$

stand for complex coefficients of the series. If $A=1$, then the circle is called the *unit circle*.

Similarly, a holomorphic function defined in the closed, simply connected, infinite *exterior* of the circle, can be developed into a *Laurent's series* which, under certain assumptions relating to the function, can be written as

$$z = f_{\text{ex}}(\zeta) = G_{-1}\zeta + \sum_{n=0}^{\infty} G_n \left(\frac{a}{\zeta}\right)^n; \quad \zeta \in [ae^{i\theta}, \infty]; \quad \theta \in [0, 2\pi], \tag{12}$$

where, again, the series converges within the indicated, infinite, closed domain, and the symbol a denotes the radius of the circle. The symbols

$$G_n; \qquad n = -1, 0, 1, 2, \dots \tag{13}$$

denote complex coefficients of the series (12).

The functions (10) and (12) will be referred to as *standard* ones.

3. Effective conformal mapping – two kinds of decomposition

From the considerations of the previous Section one could gain the impression that the task of determining the conformal mapping of a disc onto a finite domain bounded by a given contour is easy, as it reduces *simply* to the problem of determining the complex coefficients (11) of the series (10). In the case of infinite domains the same task seems to reduce to the problem of determining the coefficients (13) of the standard function (12).

Unfortunately, neither problem is at all 'easy'. On the contrary, they are both rather difficult to solve, for the following reasons:

1. Formulae for *evaluating* coefficients (11) and (13) in the case of *arbitrary* contours **do not exist**.

2. The algorithms for determining these coefficients are **non-linear**, and always involve an iterative process whose convergence has not been proved theoretically.

3. The **accuracy** of conformal mapping, understood as a suitably defined 'difference' between the given contour and the one described by the series (10) or (12), depends principally on the number of terms retained after the unavoidable truncations. This number usually has to be rather large – from several hundred to several thousand – which may cause **computational difficulties**.

Considering the strategy of solving the problem of conformal mapping as a whole, one should also keep in mind some general factors that influence the number of terms to be retained in the series (10) or (12).

The first of these factors is **the type of domain**. Namely, the *power* series (10) is rather slowly convergent on the circle bounding the domain, so that a somewhat larger number of terms is necessary in comparison with the series (12) under comparable circumstances.

A second important factor is **the shape of the given contour**. In order to get the 'feeling' of this property, one should consider the *trivial* case when the given contour is represented by a circle. Obviously, each one of the corresponding series – (11) or (13) – would in this case reduce solely to two terms: the constant and the linear one. The more the given contour differs from the circle, the more terms are needed.

It can be concluded that the most natural idea of describing a sought-after conformal mapping of a given domain by means of just one of the series (10) or (12) may turn out to be impracticable – not for theoretical, but for computational reasons. In particular, we are convinced that

the Vistula Lagoon (Fig. 1) belongs to such 'too difficult' cases, intractable
in *a single step*.

So, in order to surmount the difficulties characteristic of the one-step
approach, the idea of *decomposing* the conformal mapping under conside-
ration has been introduced instead. Two kinds of decomposition will be
applied.

Decomposition of the given domain consists in dividing it into
a number of subdomains. The need for such decomposition arises particu-
larly when the domain is elongated. This kind of decomposition is illustrated
in Fig. 4., which shows the Vistula Lagoon divided into five subdomains
by means of four rectilinear, parallel and equidistant segments denoted by
Arabic digits. Every subdomain resembles a disc more nearly than the whole
domain does.
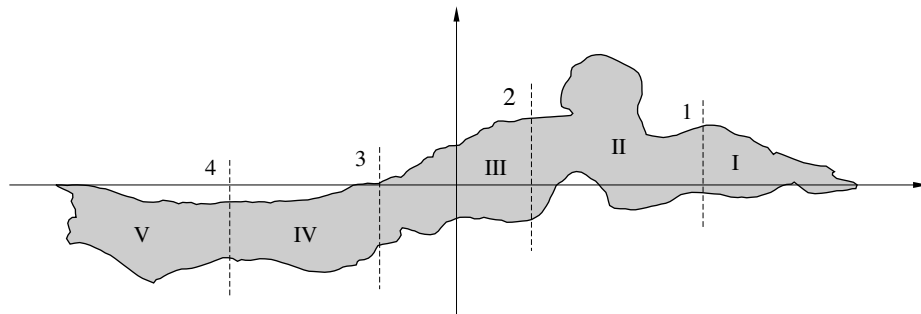
**Fig. 4.** Decomposition of the Vistula Lagoon into five subdomains

Decomposition of the conformal mapping process means that the
domain (or subdomain) under consideration is transformed onto a circular
one gradually, *step-wise*, the boundary lines of the consecutive, *intermediate*
domains tending more and more towards a circle. This is illustrated in Fig. 5,
which refers to a four-step transformation.

It starts with the 'original' domain (a in Fig. 5), which is located in the
complex z-plane. This domain is transformed by means of the function

$$\lambda_1 = F_1(z) \tag{14.1}$$

onto an intermediate one, denoted (b) in Fig. 5, and located in the λ_1-plane.
The function (14.1) is usually adopted in the form of the *Schwarz-Christoffel*
function, which will be discussed in the next Section.

Now, because conformal mapping of infinite domains is 'easier' to
execute numerically than such mapping of finite ones, the finite domain (b)
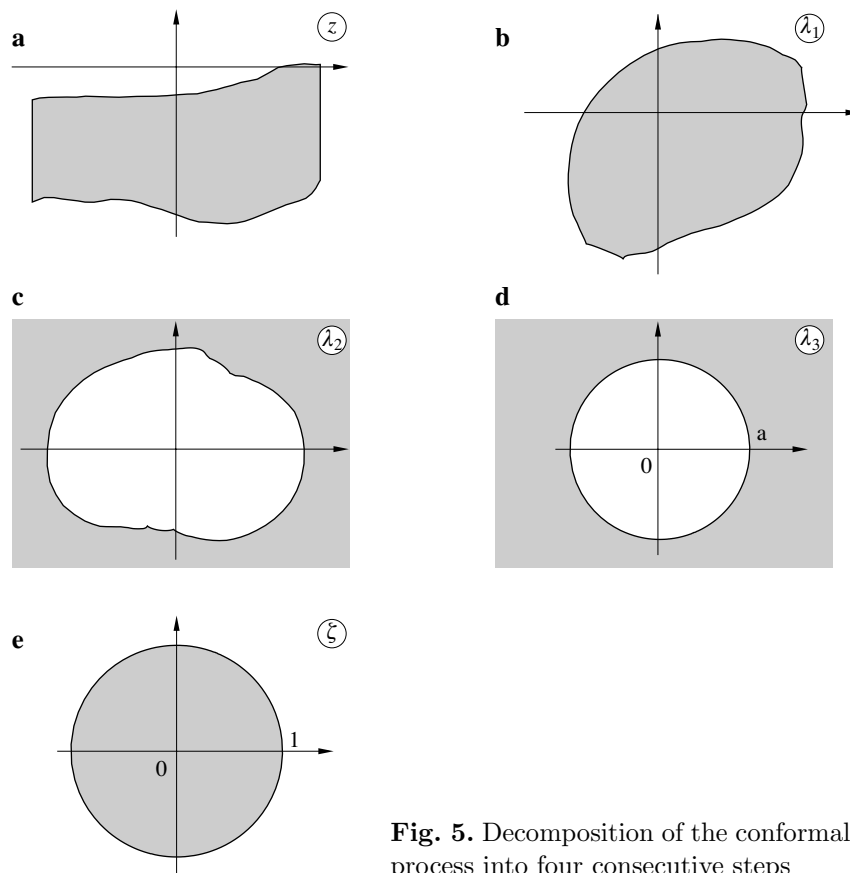
Fig. 5. Decomposition of the conformal mapping process into four consecutive steps

is transformed onto the infinite one, denoted (c) in Fig. 5. This is done by means of *inversion*, described by the function

$$\lambda_2 = F_2(\lambda_1) = \frac{D}{\lambda_1 - \lambda_1{}^*}, \tag{14.2}$$

where D denotes a complex scaling factor, and $\lambda_1{}^*$ the center of inversion. It has to lie inside domain (b).

Next, domain (c) is transformed onto the closed exterior of the circle (d) by means of the *standard* function

$$\lambda_3 = F_3(\lambda_2). \tag{14.3}$$

The symbol a will stand for the radius of this circle (cf. (12) and Fig. 5). It should be stressed that (14.3) represents the crucial element of the whole set of transformations, determining its entire accuracy.

Finally, the closed exterior of the circle (d) situated in the λ_3-plane is transformed by means of the function

$$\zeta = \frac{a}{\lambda_3} \qquad (14.4)$$

onto the *unit disc* (e), situated in the ζ-plane.

4. Functions representing consecutive mappings

In the present Section the most important functions realizing the separate steps of conformal mapping applied in this work will be set out and commented on.
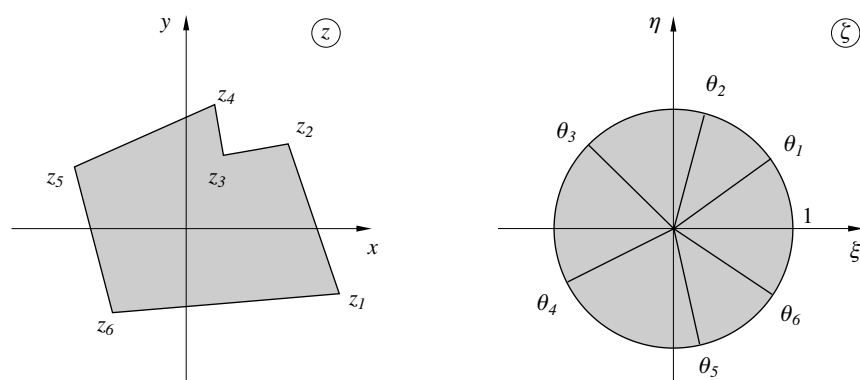
The Schwarz-Christoffel function, defined by the formula

$$z = K_0 + K_1 \int_{\zeta_d}^{\zeta_N} \prod_{n=1} (1 - \zeta e^{-i\theta_n})^{p_n} d\zeta \qquad (15)$$

transforms conformally a unit disc located in the ζ-plane onto a polygon, defined in the z-plane by means of its N vertices:

$$z_n; \qquad n = 1, 2, ..., N \qquad (16)$$

(see Fig. 6).

Fig. 6. Conformal mapping of a disc onto the interior of a polygon

In formula (15) the symbols K_0, K_1 denote complex constants, and ζ_d an initial point of integration that has to be chosen within the disc:

$$|\zeta_d| < 1.$$

The exponents p_n in (15) depend on the inner angles α_n of the polygon (not indicated in Fig. 6):

$$p_n = \frac{\alpha_n}{\pi} - 1; \qquad n = 1, 2, ..., N. \qquad (17)$$

The remaining exponents –

$$\theta_n; \qquad n = 1, 2, ..., N \qquad (18)$$

– represent counter-images of the vertices (16). They are usually referred to as *parameters of the Schwarz-Christoffel function*. The values of the parameters corresponding to an *arbitrary* polygon are not known in advance. In the case of a *regular* one, they are distributed equidistantly on the circle bounding the disc. For instance, for a square they can be assumed as given in Table 1.

Table 1. Vertices of a square, and the parameters of the corresponding *Schwarz-Christoffel* function

n	1	2	3	4
x_n	0.5	−0.5	−0.5	0.5
y_n	0.5	0.5	−0.5	−0.5
θ_n	$\frac{\pi}{2}$	π	$\frac{3}{2}\pi$	0
error	-5.6×10^{-17}	-1.1×10^{-16}	-5.6×10^{-17}	0

The problem of determining the parameters (18) for an *arbitrary* polygon is non-linear and not easy to solve, especially in the case when the contour is elongated, indented, and has a large number of vertices. However, if this number is smaller than 10, then the computer program developed by Prosnak & Klonowska (1996a) delivers very accurate solutions, the accuracy being defined as the maximum distance between a given vertex z_n and its image delivered by the function (15). For a square with sides equal to 1, the program yields the errors set out in Table 1.

According to the property mentioned before, the function (15) can be developed into a power series:

$$z = \sum_{k=0}^{K} B_k \zeta^k, \tag{19.1}$$

where the coefficients depend *explicitly* on constants of the function – especially on the parameters – and can be *evaluated* very accurately for *any number K* of the terms of the series. No iterative process is involved in their determination. Hence, it should be remembered that the series (19.1) transforms rather accurately the unit circle shown in Fig. 6 onto the corresponding polygon, provided that a sufficiently large number K is adopted. In the case of the square, an accuracy of the order of 0.0001 can be achieved only for $K \geq 4000$ (see Filchakov 1964, p. 499).

In the remainder of the present paper the 'provenience' of the series (19.1) will be ignored, and the series will be regarded merely as an *exact* function that transforms the unit circle onto a *regular* contour, very similar to the given polygon, but possessing rounded-off vertices.

The inverse of the function (19.1) can be written formally as

$$\zeta = \sum_{k=1}^{K} \tilde{B}_k z^k. \tag{19.2}$$

However, in the present work the value ζ of the inverse will always be determined numerically from (19.1), for a given value of z, with high accuracy.

Function (14.1) can be regarded as identical with (19.2). It represents the first step in all sets of step-wise conformal mappings, corresponding to the five subdomains.

In all the sets of consecutive operations just mentioned, the one involving the determination of the complex coefficients (11) of the power series (10) for a given domain, and *by means of an iterative process*, has been studiously avoided, for reasons mentioned in the previous Section (slow convergence). Instead, the finite domain under consideration (b in Fig. 5) has been transformed by means of function (14.2) onto an infinite one (c in Fig. 5).

The functions (14.2) and (14.4) hardly need any comment.

On the other hand, it should be recalled that the function mapping the exterior of a circle (d in Fig. 5) onto the infinite domain bounded by a known *Jordan* line, is sought in the form of the standard function (12), its coefficients being determined in a fairly effective iterative process developed by Prosnak & Klonowska (1996a, b). The corresponding computer program is presented in Prosnak & Klonowska (1996a).

If necessary, the already introduced *Joukowski* function (7) is also applied in our work to rectify local indentations of the contour under consideration. An example of this kind is presented in Fig. 7. The 'indented' domain, located in the z-plane, is transformed together with the inscribed *Joukowski* profile onto the ζ-plane by means of the inverse of the *Joukowski* function (7):

$$\zeta = \frac{z}{2} \pm \sqrt{\left(\frac{z}{2}\right)^2 - c^2}. \tag{20}$$

It can be easily seen in Fig. 7 that the 'indentation' does not appear in the domain so transformed. Obviously, the circle on the right hand side of Fig. 7 represents the image of the *Joukowski* profile obtained by means of the function (20).
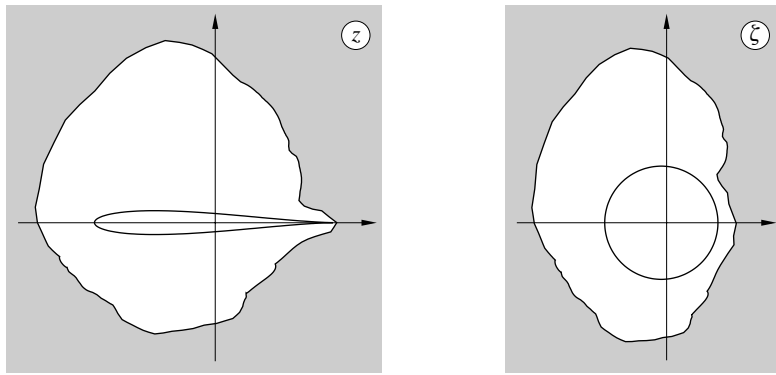
Fig. 7. Local 'rectification' of a contour by means of the *Joukowski* function

One of the existing generalisations of the *Joukowski* profile and of the *Joukowski* function has been given by Kármán & Trefftz (1918). The *Kármán-Trefftz* function can be presented in the following form:

$$\frac{z - 2c}{z + 2c} = \left(\frac{\zeta - c}{\zeta + c}\right)^m ; \qquad (0 < m \le 2). \tag{21}$$

When $m = 2$ the function reduces to the *Joukowski* one, and the angle δ between the tangents to the profile at the cusp is zero (Fig. 7). For increasing m the angle increases too, according to the relation

$$m = \frac{2\pi - \delta}{\pi}$$

between the exponent and the angle.

The function (20) transforms the circle into a *Kármán-Trefftz* profile, together with corresponding exteriors. An example is shown in Fig. 8, where the contour resembles a figure of eight, and the angle $\delta = 315°$.
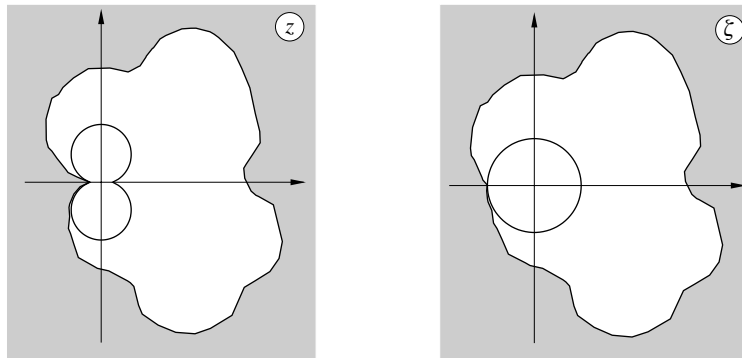
Fig. 8. Local 'rectification' of a contour by means of the *Kármán-Trefftz* function

The function is a rather powerful tool for the local rectification of contours possessing edge-like indentations.

The (almost) complete collection of 'partial' mapping functions used in the present work can therefore be listed as follows:

- the *Schwarz-Christoffel* function (15),
- the truncated power series (19.1), representing the development of the *Schwarz-Christoffel* function,
- the inverse (19.2) of the function (19.1), computed numerically as the solution of (19.1) with respect to ζ for given z,
- the function (14.2), representing the so-called inversion,
- the standard function (12), conformally mapping the infinite exterior of the circle of radius a onto the infinite exterior of a given contour,
- the *Joukowski* function (7), and the inverse (20) of this function,
- the *Kármán-Trefftz* function (21), and the inverse of this function.

Auxiliary operations, such as scaling, shifting and rotating a contour, have been omitted from the list, which can therefore be regarded as almost complete.

The functions (15) and (19) can be considered *fairly exact*. Their accuracy depends solely on that of the parameters (18), which is usually very high, as will be seen in Section 6.

In contrast, the functions (14.2), (7), (20), and (21) **are** *exact*: they contain exclusively exact constants.

On the other hand, the standard mapping function (12) must be considered *approximate*. It is truncated and contains coefficients obtained by the use of the iterative process, their accuracy depending on the number of retained terms and on the shape of the transformed domain. Hence, the accuracy of the whole step-wise conformal mapping depends mostly on the accuracy of the determination of the coefficients (13) of series (12). This property was already mentioned in Section 3.

5. Data for the conformal mapping of the Vistula Lagoon

The original data, which describe the shape of the Vistula Lagoon and are assumed to be the basis of the computations performed within the framework of the present paper, consist of a list of the rectangular coordinates of 881 discrete points on the contour of the Lagoon (Fig. 1). The list is stored at the Institute of Oceanology of the Polish Academy of Sciences under the supervision of the second author of this paper.

Following the (already introduced) decomposition of the domain, and the subsequent shifting of the subdomains thus obtained along the axis of

the abscissae, they can be presented separately, as shown in Fig. 9.
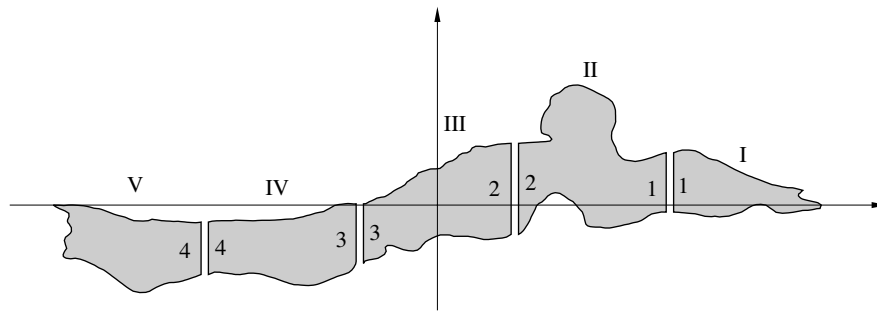
Fig. 9. The five subdomains: the result of the decomposition of the Vistula Lagoon

The four rectilinear segments separating the subdomains are defined by the following numbers of discrete points:

$$N_1 = 28; \qquad N_2 = 42; \qquad N_3 = 28; \qquad N_4 = 25. \tag{22}$$

Consequently, the total numbers of points defining consecutive subdomains are

$$N_{\mathrm{I}} = 244; \quad N_{\mathrm{II}} = 279; \quad N_{\mathrm{III}} = 225; \quad N_{\mathrm{IV}} = 186; \quad N_{\mathrm{V}} = 185. \tag{23}$$

The corresponding five lists of coordinates are also stored at IO PAN.

6. Results of conformal mapping of the Vistula Lagoon

The results of conformal mapping of the Vistula Lagoon will be presented in this Section in a *natural* way, following on from the decomposition of this domain into five subdomains, each of which can be treated independently. Hence, the presentation will refer consecutively to each one of these subdomains, and within the framework of every 'sub-presentation' the sequence of partial conformal mappings will be produced. The most decisive terms of the sequence will be shown in graphical form. In general, no numerical results will be included in the presentation, except the parameters of the *Schwarz-Christoffel* function.

The structure of most sequences resembles rather closely the general scheme shown in Fig. 5. However, one more operation occurs in the sequences relevant to the subdomains I and II.

Subdomain No. I

This subdomain is shown in Fig. 10. Its boundary is denoted by C_z, and the symbol E refers to the octagon approximating this boundary.
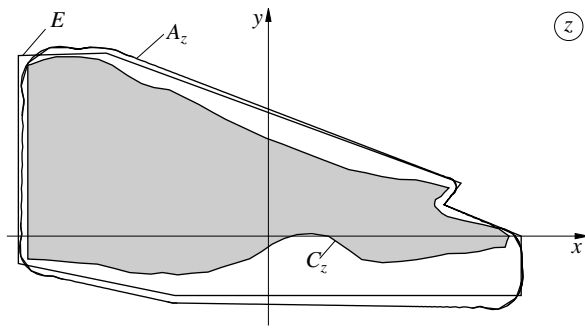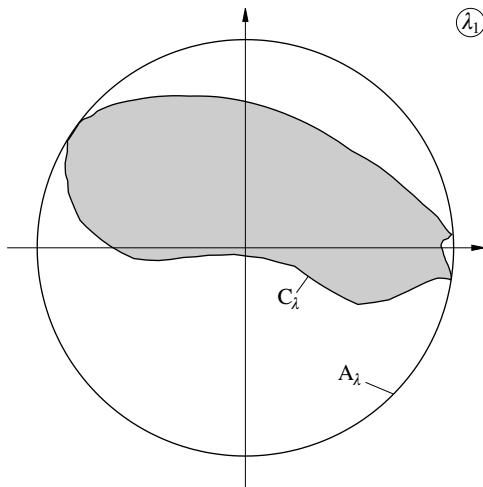
Fig. 10. The octagon and the quasi-octagon approximating the boundary of subdomain I

The parameters of the *Schwarz-Christoffel* function corresponding to the octagon, which have been computed by means of an advanced version of the computer program by Prosnak & Klonowska (1996a), are set out in Table 2.

Besides the coordinates of the vertices and the above-mentioned parameters, the Table contains errors referring to the lengths of the octagon's sides and not to positions of the vertices directly.

The third contour in Fig. 10, denoted by A_z, represents the image of the unit circle by means of the series (19.1), which contains $K = 500$ terms.

This unit circle, shown in Fig. 11 and denoted by A_λ, represents the image of the contour A_z in the λ_1-plane computed by means of the inverse (19.2) of the function (19.1).

Fig. 11. Counter-image of the quasi-octagon and of the boundary of subdomain I shown in Fig. 10

On the other hand, the contour C_z is transformed by means of the same function (19.2) into the contour bounding the finite domain in Fig. 11.
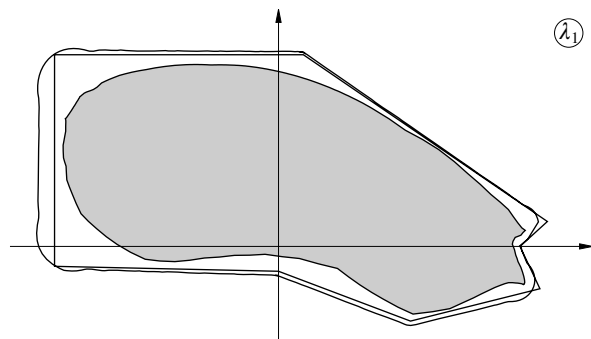
Table 2. Vertices of the octagon approximating the boundary of subdomain I (Fig. 10), and the parameters of the corresponding *Schwarz-Christoffel* function

n	1	2	3	4	5	6	7	8
x_n	0.08	−0.067	−0.104	−0.104	−0.039	0.105	0.105	0.073
y_n	0.022	0.076	0.075	−0.011	−0.025	−0.025	0.00	0.013
θ_n	3.8136	141.4944	142.9352	149.1458	163.4278	350.217	351.1182	0.00
error	-2.2×10^{-4}	-3.6×10^{-3}	-7.4×10^{-3}	-1.0×10^{-3}	-5.8×10^{-3}	-7.1×10^{-3}	-7.5×10^{-4}	0.00

Table 3. Vertices of the octagon approximating the boundary of the transformed subdomain I (Fig. 12), and the parameters of the *Schwarz-Christoffel* function

| n	1	2	3	4	5	6	7	8
$\sigma_n^{[1]}$	1.08	0.10	−0.90	−0.90	0.00	0.53	1.05	0.97
$\tau_n^{[1]}$	0.10	0.77	0.77	−0.08	−0.10	−0.30	−0.17	0.00
$\tilde{\theta}_n$	1.3928	232.1624	270.4352	274.8862	305.2365	347.9145	358.0333	0.00
error	-9.4×10^{-4}	-6.7×10^{-3}	-2.7×10^{-3}	-3.5×10^{-3}	1.7×10^{-3}	-1.4×10^{-3}	-2.6×10^{-3}	0.00

It can be seen that the domain in Fig. 11 needs at least one more transformation in order to approach the unit disc. Again, the *Schwarz-Christoffel* function has been used as the means for the additional transformation. Hence, in Fig. 12 the domain is again shown in the λ_1-plane, but this time it appears together with its 'own' approximation in the form of an *octagon*, and with the *quasi-octagon* representing the image of the unit circle by means of the series (19.1), where $K = 500$.

Fig. 12. The octagon and the quasi-octagon approximating the boundary of the intermediate domain shown in Fig. 11

The coordinates of the octagon's vertices and the parameters of the corresponding *Schwarz-Christoffel* function are given in Table 3.

By transforming the boundary shown in Fig. 12 by means of (19.2), one obtains the contour shown in Fig. 13 in the λ_2-plane; the unit circle denotes the image of the corresponding *quasi-octagon*. The domain in Fig. 13 does indeed resemble the unit disc much more than the one shown in Fig. 11.
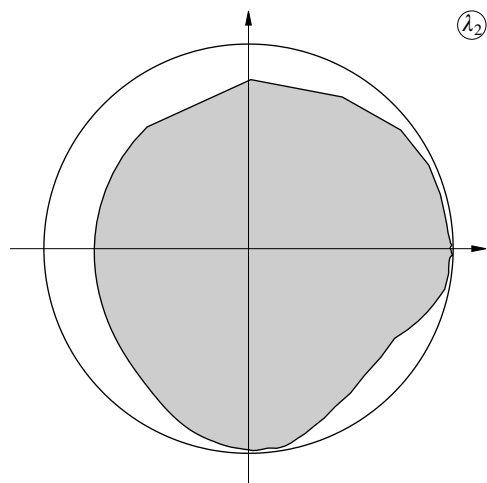
Fig. 13. Counter-image of the quasi-octagon and of the boundary shown in Fig. 12

The next step consists in transforming the finite domain (Fig. 13) onto an infinite one (Fig. 14) by means of a function similar to (14.2) and representing inversion. The function is in fact identical with (14.2), but contains differently denoted coefficients. The result is shown in Fig. 14.
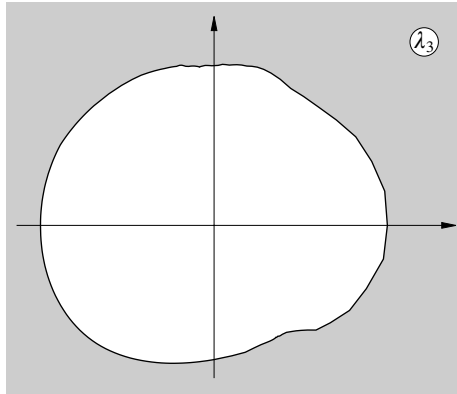
Fig. 14. Inversion of the finite domain shown in Fig. 13 onto an infinite one

Further, function (12) is applied, which transforms the infinite exterior of a circle onto the infinite exterior of the contour visible in Fig. 14. The relevant computer program (Prosnak & Klonowska 1996a) yields

$$a_{\mathrm{I}} = 0.46744; \qquad \delta_{\mathrm{I}} = 0.00469; \tag{24.1}$$

at

$$N_{\mathrm{I}} = 198; \qquad I_{\mathrm{I}} = 1000, \tag{24.2}$$

where

a_{I} – radius of the circle,

δ_{I} – maximum error of the mapping,

N_{I} – number of terms in the series (12),

I_{I} – number of nodes occurring in the iterative process for the contour shown in Fig. 14; the meaning of the nodes is explained in Prosnak & Klonowska (1996a).

The indices refer to the number of the subdomain.

The error is defined as the distance between a given point on the boundary in Fig. 14 and its image, calculated by means of function (12), which contains coefficients (13), supplied by the above-mentioned computer program.

The infinite circular domain, such as appears in Fig. 5d, is finally transformed by means of inversion (14.4) onto the unit disc, which represents the final result of the step-wise transformation of subdomain No. I. The two figures analogous to Figs. 5d, 5e are omitted for the sake of brevity.

Subdomain No. II

The step-wise conformal mapping of subdomain No. II consists of exactly the same elements as in the previous case.

The subdomain under consideration is shown in Fig. 15 together with the nonagon E_{II}^1 approximating the boundary line C_{II}^1. The *quasi-nonagon*, obtained as a map of the unit circle by means of series (19.1), with $K = 400$, is also visible in Fig. 15.
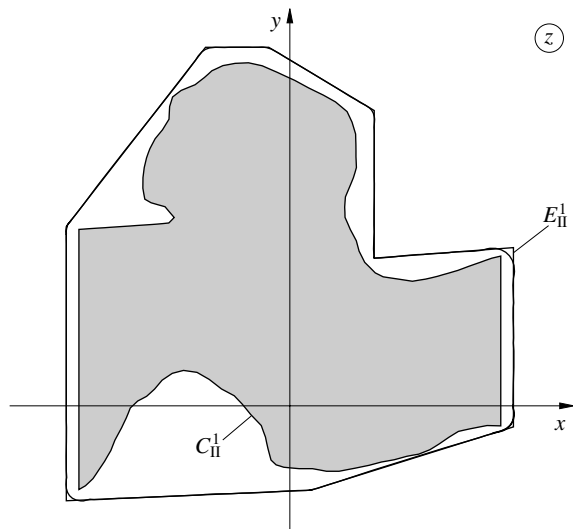
Fig. 15. The nonagon and the quasi-nonagon approximating the boundary of subdomain II

Table 4 gives the vertices and parameters of the *Schwarz-Christoffel* function.

By using the inverse (19.2) of function (19.1), one can transform Fig. 15 onto another one, shown in Fig. 16, where the unit circle represents the image of the quasi-nonagon. The domain turns out to be rather irregular, with deep indentations and several angular points. Therefore, in order to remove the irregularities, it has to be transformed again by means of the *Schwarz-Christoffel* function. Hence, as before, the domain is shown again in Fig. 17, together with its 'own' nonagon and quasi-nonagon.

Table 4. Vertices of the nonagon approximating the boundary of subdomain II (Fig. 15), and the parameters of the corresponding *Schwarz-Christoffel* function

n	1	2	3	4	5	6	7	8	9
x_n	0.040	0.040	−0.010	−0.040	−0.106	−0.106	0.010	0.106	0.106
y_n	0.070	0.140	0.170	0.170	0.085	−0.045	−0.040	−0.010	0.075
θ_n	32.7457	76.0787	85.0258	88.1418	120.7356	181.9710	279.8812	346.6041	0.00
error	-1.2×10^{-6}	-3.1×10^{-6}	-9.4×10^{-6}	3.9×10^{-6}	-2.6×10^{-6}	-2.4×10^{-6}	-5.7×10^{-7}	3.7×10^{-7}	0.00

Table 5. Vertices of the nonagon approximating the boundary of the transformed subdomain II (Fig. 17), and the parameters *of the Schwarz-Christoffel* function

| n	1	2	3	4	5	6	7	8	9
$\sigma_n^{[1]}$	0.85	0.43	0.28	0.13	−0.92	−0.27	−0.62	0.00	0.85
$\tau_n^{[1]}$	0.62	0.94	0.76	1.10	0.62	0.27	−0.50	−1.15	−0.74
$\tilde{\theta}_n$	65.6015	83.9963	99.2273	122.4778	152.360	201.8292	325.0414	343.0924	0.00
error	-1.0×10^{-5}	-1.4×10^{-5}	-1.3×10^{-5}	-5.3×10^{-6}	7.2×10^{-6}	1.1×10^{-5}	-2.9×10^{-6}	-2.9×10^{-6}	0.00
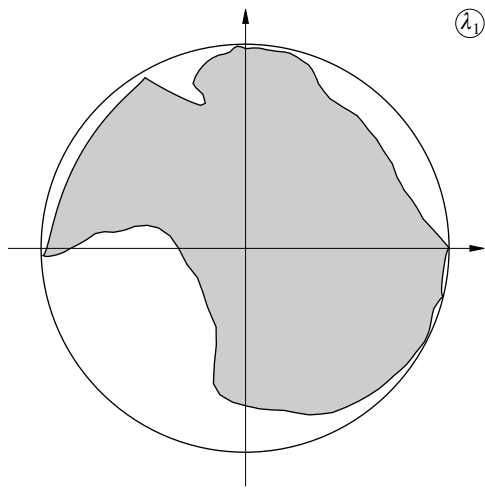
Fig. 16. Counter-image of the quasi-nonagon and of the boundary of sub-domain II shown in Fig. 15
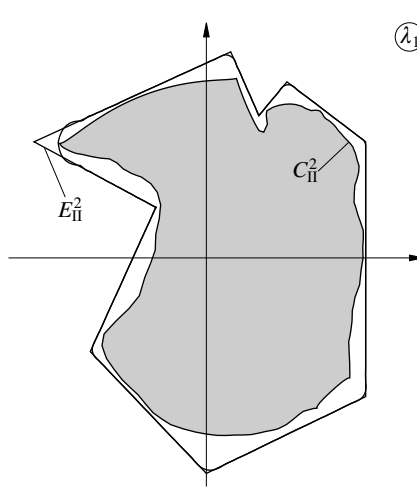
Fig. 17. The nonagon and the quasi-nonagon approximating the boundary of the intermediate domain shown in Fig. 16

The corresponding vertices and parameters of the *Schwarz-Christoffel* function are set out in Table 5.

The result of transforming Fig. 17 by means of the inverse (19.2) of the function (19.1) yields the finite domain shown in Fig. 18.
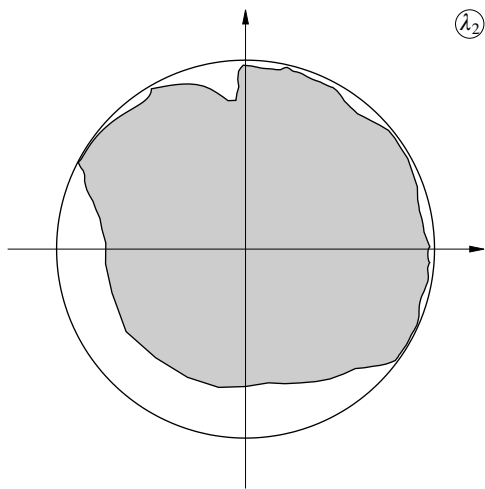
Fig. 18. Counter-image of the quasi-nonagon and of the boundary shown in Fig. 17

This domain is now transformed onto an infinite one, the resulting figure (similar to Fig. 14), however, being omitted for the sake of conciseness.

In this case the computer program (Prosnak & Klonowska 1996a) yields

$$a_{\text{II}} = 0.41407; \qquad \delta_{\text{II}} = 0.00748; \tag{25.1}$$

at

$$N_{\text{II}} = 198; \qquad I_{\text{II}} = 1000; \tag{25.2}$$

the meanings of these four symbols has already been explained.

Pictures of the infinite and the finite circular domains (cf. Fig. 5) are also omitted here. The corresponding partial mapping functions do not need any comment either.

Subdomain No. III

The transformation of this subdomain is even simpler than that of the two previous ones, because only *single* mapping by means of the *Schwarz-Christoffel* function turns out to be necessary. Consequently, the structure of the step-wise transformation is here entirely identical with the general scheme shown in Fig. 5.

Subdomain No. III is shown in Fig. 19, together with the octagon approximating its boundary C_{III}, and with the quasi-octagon representing the image of the unit circle obtained by means of series (19.1) with $K=500$.
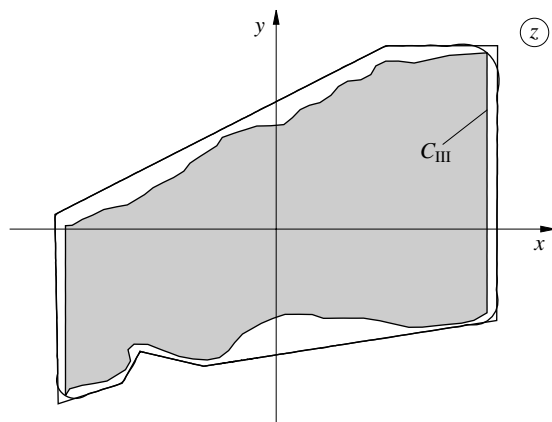
**Fig. 19.** The octagon and the quasi-octagon approximating the boundary of subdomain III

The coordinates of the octagon's vertices shown in Fig. 19, and the parameters of the corresponding *Schwarz-Christoffel* function can be found in Table 6.

Table 6. Vertices of the octagon approximating the boundary of subdomain III (Fig. 19), and the parametrs of the corresponding *Schwarz-Christoffel* function

n	1	2	3	4
x_n	−0.0113	−0.0996	−0.0847	−0.0684
y_n	0.1046	0.0875	0.0593	0.0536
θ_n	122.0899	154.1781	157.1835	167.5624
error	4.7×10^{-8}	1.9×10^{-5}	2.1×10^{-5}	6.7×10^{-6}

n	5	6	7	8
x_n	−0.0701	−0.0246	0.1039	0.0947
y_n	0.0227	−0.1105	−0.0883	−0.0361
θ_n	225.7115	346.3073	357.4425	0.00
error	4.5×10^{-7}	2.7×10^{-6}	-1.4×10^{-6}	-2.2×10^{-16}

The image of subdomain III obtained by means of (19.2) appears as a finite domain in Fig. 20. This domain is sufficiently regular and can be transformed *directly* onto an infinite domain – see Fig. 5.
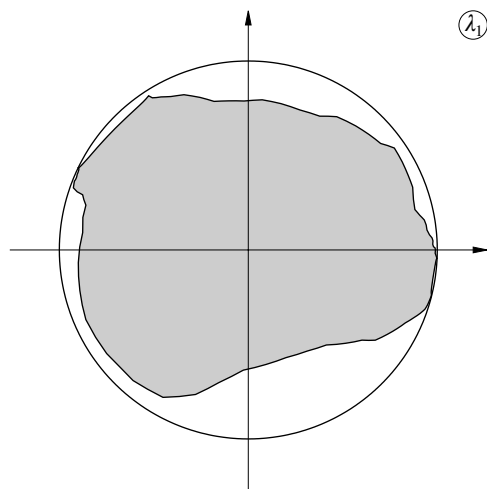
Fig. 20. Counter-image of the quasi-octagon and of the boundary of subdomain III shown in Fig. 19

As before, the standard function (12) is applied in order to map the domain thus obtained onto an infinite *circular* one, the computer program (Prosnak & Klonowska 1996a) yielding the following results:

$$a_{\text{III}} = 0.43354; \qquad \delta_{\text{III}} = 0.00705; \tag{26.1}$$

at

$$N_{\text{III}} = 198; \qquad I_{\text{III}} = 1000. \tag{26.2}$$

The image of Fig. 20 representing the infinite domain (see Fig. 5d), as well as the circular domains, have been omitted in order to save space.

Subdomain No. IV

This subdomain is shown in Fig. 21 in the same manner as the three previous ones. It contains the quadrilateral, approximating boundary of the subdomain; it also contains the *quasi-quadrilateral*. This last curve represents the image of the unit circle obtained by means of the inverse (19.2) of series (19.1), where $K = 400$.
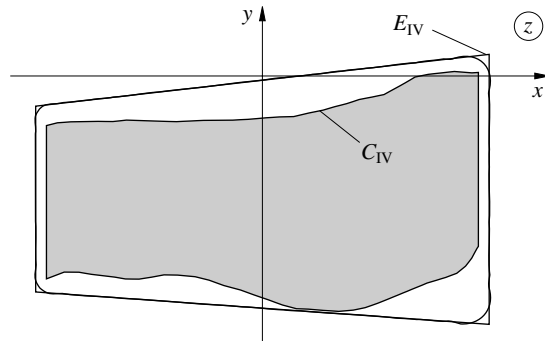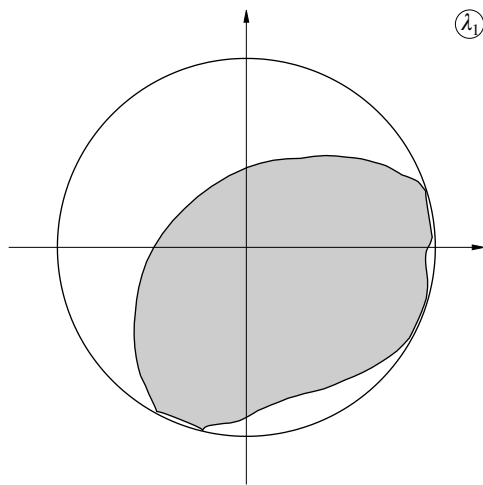

Fig. 21. The quadrilateral and the quasi-quadrilateral approximating the boundary of subdomain IV

The coordinates of the vertices and parameters of the corresponding *Schwarz-Christoffel* function are set out in Table 7.

Table 7. Vertices of the quadrilateral approximating the boundary of subdomain IV (Fig. 21), and the parameters of the corresponding *Schwarz-Christoffel* function

n	1	2	3	4
x_n	0.105	−0.105	−0.105	0.105
y_n	0.010	−0.014	−0.100	−0.115
θ_n	17.5681	240.9084	256.6475	0.00
error	-1.2×10^{-10}	-7.8×10^{-12}	-1.0×10^{-10}	0.00

As before, the counter-image of the quasi-quadrilateral and of the boundary of the intermediate finite domain are shown in Fig. 22.

Fig. 22. Counter-image of the quasi-quadrilateral and of the boundary of subdomain IV shown in Fig. 21

This result is transformed again by means of the function (14.2), yielding the infinite domain shown in Fig. 23.
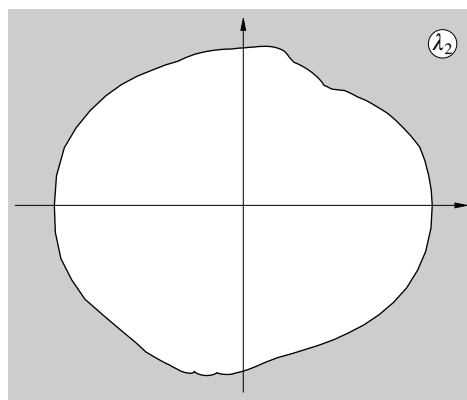
Fig. 23. Inversion of the finite domain shown in Fig. 22 onto an infinite one

The results of the conformal mapping of this last domain onto the infinite, circular one provided by the computer program (Prosnak & Klonowska 1996a) contain

$$a_{\mathrm{IV}} = 0.46050; \qquad \delta_{\mathrm{IV}} = 0.00695; \qquad\qquad (27.1)$$

at

$$N_{\mathrm{IV}} = 180; \qquad I_{\mathrm{IV}} = 1000. \qquad\qquad (27.2)$$

As previously, the auxiliary transformations of the infinite domain, such as rotation, shifting, translating, as well as the use of the *Joukowski* function, which have been applied to render mapping by means of the standard

function (12) as effective as possible, are omitted in their entirety. Of course, they have been saved in the relevant files, which contain the full numerical results of every set consisting of the step-wise conformal mappings. Pictures of the two corresponding circular domains are again omitted.

Subdomain No. V

As in the previous case, the fundamental results are contained in three Figures and one numerical Table.

Subdomain V, together with the approximating pentagon and quasi-pentagon, is shown in Fig. 24.
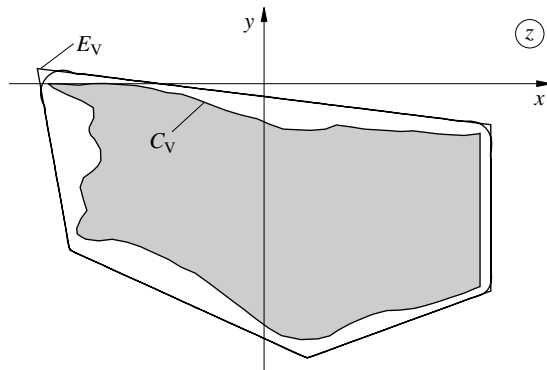
Fig. 24. The pentagon and the quasi-pentagon approximating the boundary of subdomain V

The coordinates of the pentagon's vertices as well as the parameters of the corresponding *Schwarz-Christoffel* function are given in Table 8.

Table 8. Vertices of the pantagon approximating the boundary of subdomain V (Fig. 24), and the parameters of the corresponding *Schwarz-Christoffel* function

n	1	2	3	4	5
x_n	−0.105	−0.090	0.020	0.105	0.105
y_n	0.007	−0.077	−0.127	−0.096	−0.019
θ_n	134.4787	158.1882	314.4368	349.8031	0.00
error	-7.5×10^{-5}	-6.5×10^{-5}	-3.4×10^{-5}	9.2×10^{-6}	0.00

The image of subdomain V, obtained by means of (19.2), is shown in Fig. 25. The number of terms in (19.1) $K = 400$.
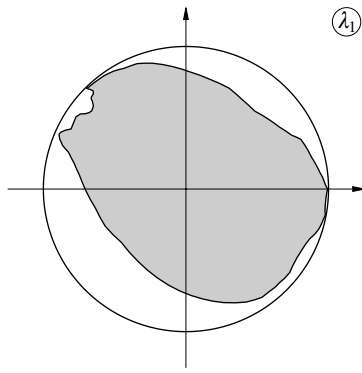
Fig. 25. Counter-image of the quasi-pentagon and of the boundary of subdomain V shown in Fig. 24
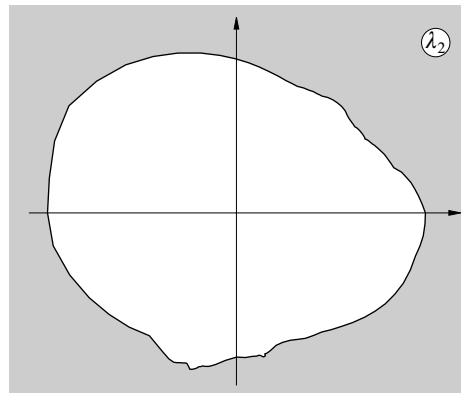
**Fig. 26.** Inversion of the finite domain shown in Fig. 25 onto an infinite one

Finally, the result of transforming the last-mentioned Figure by means of (14.2) is shown in Fig. 26.

The infinite domain so obtained is bounded by an insufficiently regular contour. Therefore, it had to be rectified locally by means of the *Joukowski* function applied twice. Moreover, the *Kármán-Trefftz* function (21) has been used for the same purpose. Being purely auxiliary, these operations can be safely omitted here without any loss of clarity.

The concluding comment can be expressed as follows.

It has been shown in this Section that every single subdomain of the Vistula Lagoon (Fig. 9) can be transformed step-wise onto a unit disc. Therefore, the set of five such discs (Fig. 27) represents the sought-after *computational* or *canonical domain* of this Lagoon. This domain is shown in Fig. 27, the images of the subdomains being denoted by Roman numerals. The arcs marked with Arabic digits represent images of the rectilinear segments shown in Fig. 9 and are denoted in the same manner. These arcs are very important: they represent *connections* between consecutive discs, and appropriate *continuity conditions* have to be imposed on them if a partial differential problem is to be formulated in the final computational domain.

The unit circles in Fig. 27 are denoted by the dashed lines. The continuous ones refer to the final results of the corresponding sets of the consecutive mappings under consideration. The discrepancy between these two lines gives some idea of the accuracy of the whole mapping process.
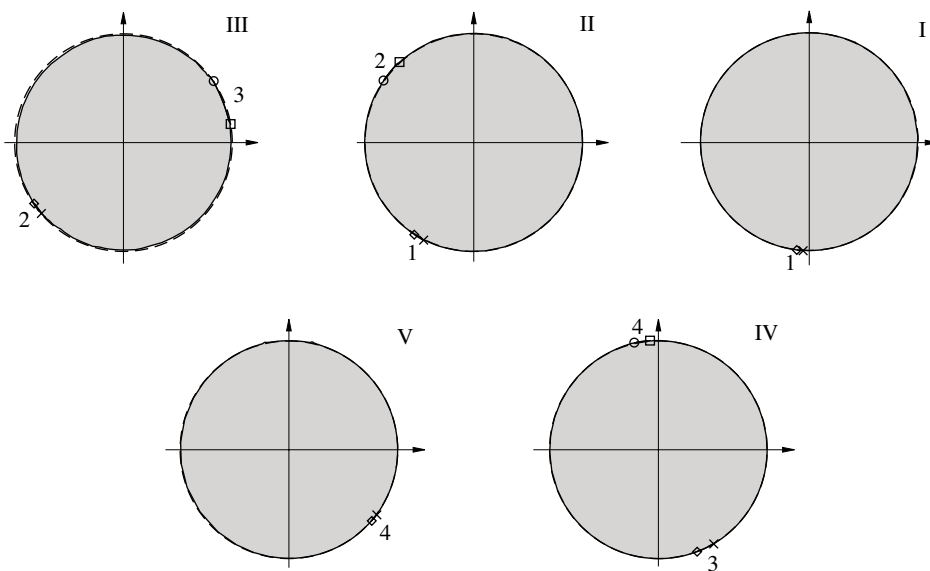
Fig. 27. The final result of all step-wise conformal mappings: a set of five unit discs

7. Conclusions and comments

It has been demonstrated that conformal mapping of simply connected domains, which has theoretically ensured existence and univalence, can be determined *effectively* even in the case of such a 'computationally difficult' domain as the Vistula Lagoon. The success is undoubtedly founded on the application of two decompositions: that of the domain to be transformed, and that of a single mapping into a set of simple ones.

The determination of such conformal mapping is nevertheless a task which requires intimate knowledge of the subject, long experience, and – quite simply – a lot of patience. The last of these virtues is particularly valuable during the gradual transformation of an infinite domain, by means of local rectifications, onto a sufficiently regular one that can be easily and accurately transformed onto a circular domain by means of the standard mapping function (12). Nevertheless, all this is usually rather time-consuming and tedious.

However, the *universality* of conformal mapping should be emphasized as one of the benefits of the transformation. Namely, the results concerning a particular domain *can be used to solve any partial differential problem* formulated in this domain as the domain of solution. This is one of the reasons why we have refrained from formulating a particular hydrodynamical problem.

The full results obtained during this research are stored at the Institute of Oceanology of the Polish Academy of Sciences. They have been carefully selected in order to make this paper as concise as possible. On the other hand, however, we have kept in mind the traditional rule that published results must be suitable for checking by the interested reader. We hope that the graphical results contained in Figs. 10 to 27, as well as the numerical ones in Tables 2 to 8, still satisfy this condition. However, we believe that any further truncation of the results will not guarantee such a possibility.

The application of these results to the solution of the partial differential problems occurring in Oceanology seems to be rather promising. In particular, the transformation of independent variables by means of conformal mapping, often feared as being complicated, is in fact rather easy. Ready (or almost ready) formulae can be taken from Prosnak & Klonowska (1996a).

Just one possible extension of this work should be mentioned.

It consists in taking into account *multiply connected* domains, defined in Section 1 rather informally as 'domains with islands'. Suitable theorems on the existence and univalence of the mapping functions, analogous to (10) and (12), have also been derived by *Koebe*. There also exist corresponding computer programs (Prosnak & Klonowska 1996a). An example concerning a 'lake' with three 'islands', transformed onto a multiply connected rectangle, can also be found in Prosnak & Klonowska (1996a).

Finally, it should be mentioned that applying the decomposition of multiply connected domains would probably always allow one to deal solely with simply connected subdomains.

Acknowledgements

References

Catewicz Z., Jankowski A., 1983, *H–N model of steady circulations in the Vistula Bay*, [in:] *Fundamentals of economics in the marine environment*, Ossolineum, Wrocław, 340 pp., (in Polish).

Filchakov P. F., 1964, *Approximate methods of conformal mappings*, Nauk. Dumka, Kiyev, 531 pp., (in Russian).

Kármán Th. von, Trefftz E., 1918, *Potential-Strömung um gegebene Tragflügelquerschnitte*, Zeitschrift für Flugtechnik und Motorluftschiffahrt, H. 17 u. 18, 9, 111–116.

Lin B., Chandler-Wilde S. N., 1996, *A depth-integrated 2D coastal and estuarine model with conformal boundary-fitted mesh generation*, Int. J. Num. Meth. Fluids, 23, 819–846.

Malebranche N., 1707, *Méditations chrétiennes et métaphysiques*, Chez Leonard Plaignard, Lyon, p. 131.

Prosnak W. J., Klonowska M. E., 1996a, *Introduction to numerical fluid mechanics. Part B: conformal mapping*, Ossolineum, Wrocław, 998 pp., (in Polish).

Prosnak W. J., Klonowska M. E., 1996b, *On an effective method for conformal mapping of multiply connected domains*, Acta Mech., 119, 35–52.

Schinzinger R., Laura P. A. A., 1991, *Conformal mapping: methods and applications*, Elsevier, Amsterdam, 581 pp.